Thermodynamic lubrication in the elastic Leidenfrost effect

Jack Binysh,[1] Indrajit Chakraborty,[2] Mykyta V. Chubynsky,[2] Vicente Luis Díaz Melian,[3] Scott R. Waitukaitis,[3] James E. Sprittles,[2] and Anton Souslov[1, *]

[1] *Department of Physics, University of Bath, Claverton Down, Bath BA2 7AY, United Kingdom*
[2] *Mathematics Institute, University of Warwick, Coventry CV4 7AL, United Kingdom*
[3] *IST Austria, Am Campus 1, Klosterneuberg, Austria*

(Dated: Tuesday 5th September, 2023)

The elastic Leidenfrost effect occurs when a vaporizable soft solid is lowered onto a hot surface. Evaporative flow couples to elastic deformation, giving spontaneous bouncing or steady-state floating. The effect embodies an unexplored interplay between thermodynamics, elasticity, and lubrication: despite being observed, its basic theoretical description remains a challenge. Here, we provide a theory of elastic Leidenfrost floating. As weight increases, a rigid solid sits closer to the hot surface. By contrast, we discover an elasticity-dominated regime where the heavier the solid, the higher it floats. We show that this elastic regime is characterized by Hertzian behavior of the solid's underbelly and derive how the float height scales with materials parameters. Introducing a dimensionless elastic Leidenfrost number, we capture the crossover between rigid and Hertzian behavior. Our results provide theoretical underpinning for recent experiments, and point to the design of novel soft machines.

The elastic Leidenfrost effect is a largely unexplored class of Leidenfrost physics, involving the vaporization of soft solids [1–5]. In the typical case of the liquid Leidenfrost effect, a fluid droplet hovers above a heated surface, cushioned by a gap layer of its own vapor. The basic physics of this scenario is extensively explored [6–12]: capillarity and gravity determine the droplet's geometry and how high it floats above the hot surface [6–10]. These advances have enabled the discovery of new effects, such as self-propelled droplets [11] and controlled wetting [13], as well as the design of new applications, for example heat exchangers [14, 15]. The typical description of Leidenfrost physics combines fluid flow and phase change, but neglects elastic deformation entirely. In one extreme, liquid Leidenfrost drops have no elastic response at all. In the other extreme, rigid sublimable solids (such as dry ice [16–18]) do not change shape when levitating above a hot surface.

When the levitated object is soft and elastic, striking phenomena result. For example, a water-saturated hydrogel lowered onto a hot surface either bounces spontaneously [1, 2] or floats on its own vapor layer [3]. Figure 1(a) shows an example of floating behavior for a sphere of radius 7 mm. These effects may appear superficially similar to the phenomenology of liquids [9, 12], but their physical origin is fundamentally different. The characteristic feature of both bouncing and floating is that the excess pressure in the vapor layer (of order kPa) is sufficiently large to elastically deform the solid [1].

The phase change occurring under the soft solid provides an intrinsic source of *thermodynamic* lubrication. This is in contrast to the *soft* lubrication problem [19–27], in which lift forces are generated when two lubricated elastic objects (for example, mammalian joints [24]) move over one another. Understanding the interplay between elasticity and flow is crucial to the design of a variety of soft devices [28–33]. If no relative motion is present, lift forces are only possible due to vaporization. However, phenomena that combine thermodynamics and large solid-body deformations, exemplified by elastic Leidenfrost physics, remain unexplored.

To fully realize the scope of elastic Leidenfrost physics, both at a fundamental level and for the potential design of soft devices, a theoretical description of the basic mechanism is required. Despite experimental observation, this description remains a challenge. In particular, there is currently no theory which explains how three-dimensional elasticity determines either the gap height of the soft solid or its shape in the floating regime.

In this Letter, we overcome this challenge by marrying soft lubrication theory with thermodynamic phase change, to formulate the first description of elastic Leidenfrost floating. By varying a single dimensionless parameter, we discover a transition from rigid behavior to an elasticity-dominated regime described by Hertzian contact mechanics. Using asymptotic analysis and finite element simulations, we quantify this Hertzian limit via scaling laws for the gap height with sphere radius and elastic modulus. Our asymptotic theory reveals the existence of two distinct scalings of the height: the first in a contact region well underneath the solid, and the second in an ever-narrowing neck region [see Fig. 1(b)]. Our results demonstrate how to tailor float height via materials properties, and offer a solid theoretical basis for exploring more complex elastic Leidenfrost phenomena [1]. This theory lays the groundwork for combining elasticity, phase change, and flow to design novel soft machines.

For a vaporizable elastic sphere of radius R, with Young's modulus E and Poisson ratio ν (Fig. 1), we show that the gap height depends on materials parameters solely through a dimensionless *elastic Leidenfrost*

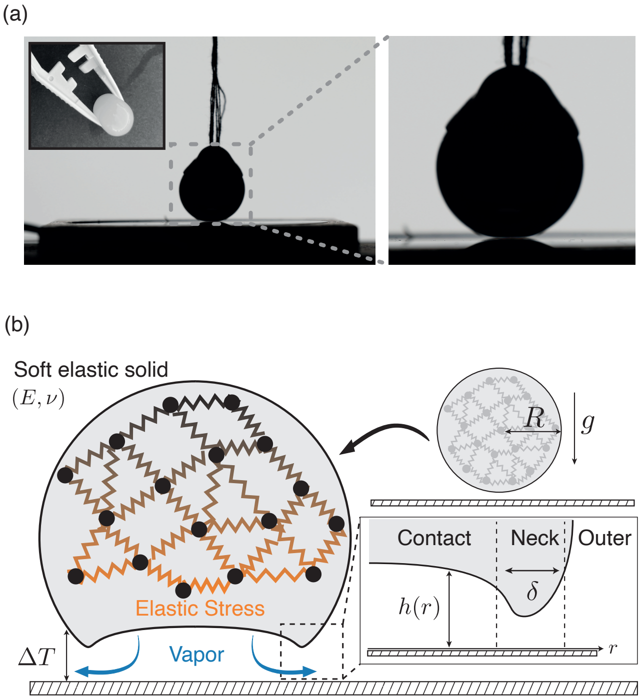

FIG. 1: **Thermodynamic lubrication in the elastic Leidenfrost effect**. (a) A soft elastic hydrogel sphere of radius $R = 7\,\mathrm{mm}$ hovers above a hot surface ($\Delta T = 115\,°\mathrm{C}$). Due to evaporative phase change, the weight of the solid is balanced by vapor flux from its underbelly, which establishes a steady gap height. Inset shows the hydrogel in daylight, squeezed by tweezers. (b) Elastic deformation from an initially spherical shape sets up a stress distribution in the soft solid. This elastic stress competes with vapor pressure to determine the shape of the solid's underbelly and the gap height. **Inset:** Our theory predicts distinct scaling laws in three regions: a contact region well under the soft solid, an outer region, and a narrow neck region of width δ.

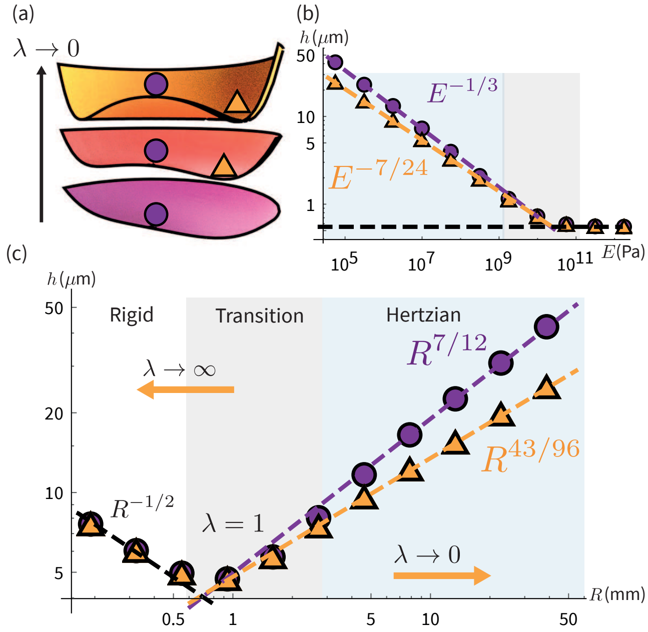

FIG. 2: **Gap height scaling laws**. (a) As the soft solid approaches the Hertzian limit $\lambda \to 0$, its underbelly develops a neck region (orange triangle), with a height scaling law distinct from that of the contact region (purple circle). Surfaces shown correspond to successive underbelly profiles as λ decreases, with the vertical axis rescaled for clarity. (b–c) Finite element simulations (markers) verify our analytically predicted gap height scaling laws (lines) for the contact and neck regions: $h \sim E^{-1/3}R^{7/12}$ in the contact region, and $h \sim E^{-7/24}R^{43/96}$ in the neck. Black lines show analytic predictions for a geometrically rigid sphere. Panel (b) shows scaling with Young's modulus E, panel (c) with sphere radius R. We find three regimes of behavior: Rigid ($\lambda \to \infty$), Transition ($\lambda \sim 1$), and Hertzian ($\lambda \to 0$). In panel (b), $R = 40\,\mathrm{mm}$. In panel (c), $E = 50\,\mathrm{kPa}$. All other materials parameters are as in Ref. [3], reproduced in the SM [34].

number,

$$\lambda = \frac{2\pi}{3}\left[\frac{4E}{3(1-\nu^2)}\right]^{4/3} \Pi_0\, F^{-7/3} R^{8/3}. \qquad (1)$$

Equation (1) encapsulates geometry, elasticity, and fluid flow. Here, $F = (4\pi/3)\rho_s g R^3$ is the solid's weight, with ρ_s its density and g the gravitational acceleration. The typical force scale in the vapor layer, Π_0, is where temperature and vapor properties enter λ, and is described further below. As $\lambda \to \infty$, we recover the height scaling law of a rigid solid (or small liquid drop [7]). As $\lambda \to 0$, however, we discover scaling laws distinct from both the rigid and the liquid Leidenfrost cases, corresponding to an asymptotically Hertzian behavior of the solid's underbelly. In this Hertzian regime, the gap height h scales as

$$h \sim \Pi_0^{1/4} E^{-1/3} R^{1/3} F^{1/12}. \qquad (2)$$

Taking the load to be proportional to the volume in Eq. (2), $F \sim R^3$, we find the height scaling $h \sim R^{7/12}$. Counter-intuitively, the heavier the soft solid, the higher it floats. A crossover between the rigid and Hertzian scaling laws occurs at the value $\lambda \sim 1$. A natural set of experimentally accessible parameters is provided by recent work on hydrogel spheres [3] [see also Fig. 1(a)], in which the radius R is on the order of mm–cm and the modulus $E \sim$ kPa. Taking parameters from Ref. [3] (reproduced in the Supplementary Material (SM) [34]) gives $\lambda \sim 10^{-5}$, well into the regime of Hertzian scaling.

To derive Eqs. (1–2), we now formulate a theory of thermodynamic lubrication coupled to elastic deformation of the solid. Figure 1(b) shows a schematic of the soft solid floating above a hot surface. The heated surface is held at a temperature difference ΔT above the vaporization threshold of the solid, causing the solid's underbelly to evaporate and open a thin vapor gap. To describe vapor flow, we note that the gap height is significantly smaller than the lateral scale of the underbelly. We use the lubrication approximation of the Navier-Stokes equations [10, 23], which neglects the vertical component of flow. In this approximation, the (axisymmetric) height profile $h(r)$ in Fig. 1(b) and the pressure in the vapor layer $P(r)$ are related through

$$\frac{1}{r}\frac{d}{dr}\left(r\frac{\rho h(r)^3}{12\eta}\frac{dP(r)}{dr}\right) = -\frac{\kappa\Delta T}{Lh(r)}. \tag{3}$$

Equation (3) expresses continuity: the pressure gradient under the solid establishes a Poiseuille flow with mass flux $\sim (\rho/\eta)h^3\nabla P(r)$, where η and ρ are the viscosity and density of the vapor. This flux is balanced by a Leidenfrost source term $-\kappa\Delta T/Lh(r)$, describing conduction-dominated evaporation from the solid's underbelly [10]. Here, κ is the vapor thermal conductivity and L is the latent heat of vaporization. This source term is where thermodynamic phase change enters the problem. It stands in contrast to soft lubrication theory [23–26] where no mass source is allowed, and flow can only be driven by externally imposed conditions.

For a steady gap height, integrated vapor pressure must balance the total weight F of the solid. If the pressure P acts over a lateral length scale l characteristic of the solid's underbelly, we have the scaling $F \sim Pl^2$. A scaling analysis of the lubrication equation (3) relates P, l, and gap height h as $P \sim \Pi_0 l^2/h^4$, where we define the vapor force scale $\Pi_0 \equiv \kappa\Delta T\eta/L\rho$. Using this pressure relation in the total force balance gives

$$F \sim \Pi_0 \left(\frac{l}{h}\right)^4. \tag{4}$$

For a given load F, Eq. (4) specifies h in terms of an unknown lateral scale l. The crucial question is then: what is the correct choice of l?

We postulate that there are two choices of l, giving two possible gap height scaling laws. The ratio of these two length scales will define λ. The first choice is for a completely rigid sphere, neglecting elasticity: $l_S = \sqrt{hR}$ [24]. Using this choice in Eq. (4) yields a gap height $h \sim \sqrt{\Pi_0/FR}$. Taking the load to scale with the volume, $F \sim R^3$, we re-derive the height scaling law for rigid spheres, $h \sim R^{-1/2}$. This scaling applies whenever geometric deformation can be neglected [7]. Intuitively, balancing an increasing radius R (i.e., an increasing weight) requires more vapor flux, and so the solid must sit closer to the heated surface.

Scaling laws unique to elastic Leidenfrost floating result from a different choice of lateral length scale l, arising from linear elasticity theory and Hertzian contact mechanics [35–37]. When an elastic sphere of Young's modulus E is placed in direct contact with a hard surface, a circular indentation results, with radius $l_H \sim (FR/E)^{1/3} \sim R^{4/3}$. In the SM [34], we show that this lateral scale also applies to our lubrication problem. The total vapor thrust then scales as the ratio $(l_H/h)^4$, but the total load scales as the volume R^3, resulting in a float height given by the balance $h \sim l_H/R^{3/4} \sim R^{7/12}$. The full scaling law given by Eq. (2), including all materials parameters, is derived in the SM [34] directly from the integro-differential system describing the coupling between elasticity and lubrication flow. Intuitively, as radius increases, elastic deformation of the solid's underbelly gives a rapidly increasing contact area over which evaporative thrust is generated. This increasing thrust outcompetes the increasing weight, leading to the counter-intuitive increase of gap height with radius R.

If length scales l_S and l_H characterize two distinct scaling regimes for the gap height, crossover between regimes is quantified by the ratio l_S/l_H. This motivates the expression for the elastic Leidenfrost number λ as

$$\lambda = \frac{2\pi}{3}\left(\frac{l_S}{l_H}\right)^4, \tag{5}$$

which is equivalent to Eq. (1) when written in terms of materials parameters. In the SM [34], we show that non-dimensionalizing the combined equations of linear elasticity and the lubrication equation (3) yields λ as the single dimensionless number governing the floating regime. Intuitively, λ compares the length scales over which the vapor pressure causes elastic deformation. When $\lambda \to \infty$, $l_S \gg l_H$ and vapor pressure is too small to cause appreciable elastic deformation. By contrast, when $\lambda \to 0$, $l_S \ll l_H$ and Hertzian elasticity dominates.

We have predicted that the dimensionless parameter λ mediates the crossover between rigid behavior and our scaling law, Eq. (2). We now test these predictions. To do so, we numerically solve for a series of profiles for the gap height $h(r)$ and for the pressure $P(r)$, across a range of sphere radii and Young's moduli. A finite element method [38, 39] is used to obtain elastic deformations by solving the primitive equations of linear elasticity throughout the 3D solid. This elastic solver is coupled to a numerical solution of the axisymmetric lubrication equation (3) to give a closed system in height $h(r)$ and pressure $P(r)$. Our finite element approach, described further in the SM [34], bypasses the assumptions made in Hertzian contact theory, i.e., the use of a half-space elastic solution for a curved boundary and a parabolic approximation to the solid's underbelly. These numerics allow us to probe the limits of validity for our theory and to test the universality of our scaling predictions in terms of λ.

In Fig. 2, we show the gap height in the contact region, $h(r = 0)$, against radius R and modulus E. Parameters not varied are fixed to natural experimental values for the hydrogel spheres used in, for example, Ref. [3]. We find a clear crossover between two distinct regimes of behavior occurring at $\lambda \sim 1$, with agreement between our predicted scaling laws, Eq. (2), and those found in

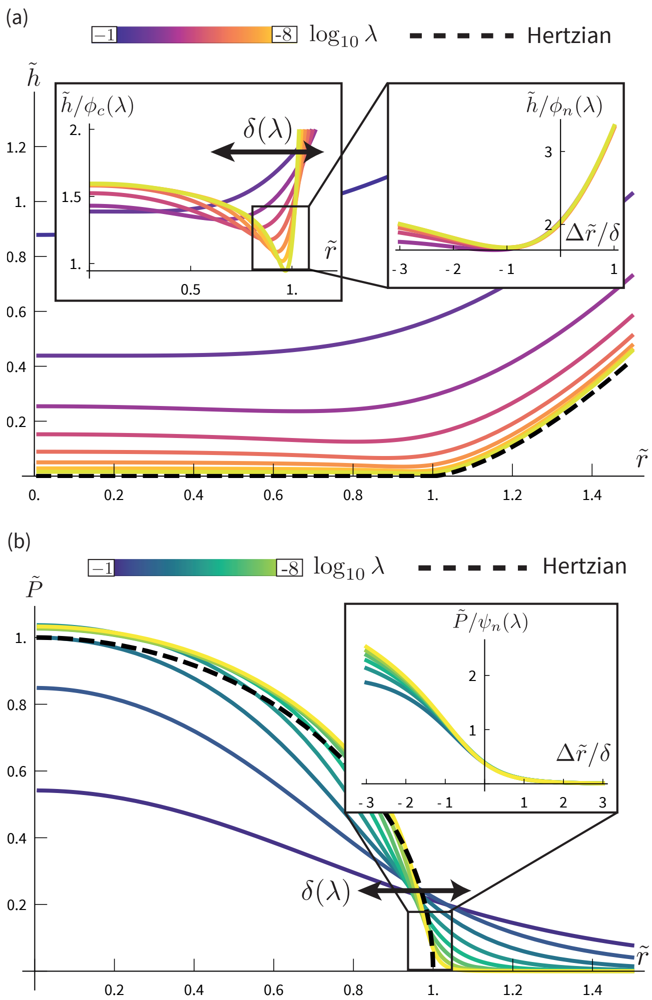

FIG. 3: **Collapsing to the Hertzian Limit.** Nondimensionalized (a) height $\tilde{h}$ and (b) pressure $\tilde{P}$ profiles, obtained from finite element simulations. Both height and pressure approach the Hertzian dry contact solutions (black dashed lines) as $\lambda \to 0$. Deviations are confined to a λ-dependent neck region, of width $\delta(\lambda)$. **Insets**: Our scaling law for the height profile in the contact region, $\phi_c(\lambda) = \lambda^{1/4}$, breaks down in the neck (a, left). Instead, our asymptotic theory predicts the collapse of profiles in the neck region when the radius $\Delta\tilde{r} \equiv \tilde{r} - 1$ is rescaled by $\delta(\lambda) = \lambda^{3/16}$, the height by $\phi_n(\lambda) = \lambda^{9/32}$ (a, right) and the pressure by $\psi_n(\lambda) = \lambda^{3/32}$ (b, right).

simulation. However, our numerical results also reveal a neck region at the edge of contact [Fig. 2(a)], which develops as the solid transitions into the Hertzian regime. The height of this neck follows a distinct scaling law, not captured by the analysis above.

To investigate this neck region further, in Fig. 3 we plot the full height [Fig. 3(a)] and pressure [Fig. 3(b)] profiles under the soft solid, non-dimensionalized by the Hertzian scales: $\tilde{r} = r/l_H$, $\tilde{h} = hR/l_H^2$, $\tilde{P} = (2\pi l_H^2/3F)P$. As $\lambda \to 0$, we note that both height and pressure profiles approach their Hertzian limits, $\tilde{h}(\tilde{r}) = (\tilde{r}-1)^{3/2}$ for $\tilde{r} \gtrsim 1$, and $\tilde{P}(\tilde{r}) = \sqrt{1-\tilde{r}^2}$ for $\tilde{r} < 1$ [36], except in a boundary layer of width $\delta(\lambda)$ located at $\tilde{r} = 1$. The discrepancy in the height data becomes clearer when we rescale $\tilde{h}$ by the contact scaling law Eq. (2). We show in the SM [34] that Eq. (2) corresponds to the dimensionless scaling law $\tilde{h}(\tilde{r} = 0) \sim \phi_c(\lambda)$, where $\phi_c(\lambda) = \lambda^{1/4}$. As shown in the left inset of Fig. 3(a), this law collapses data in the contact region, but fails in the neck $\delta(\lambda)$. The reason for this discrepancy is that the Hertzian dry contact solutions are singular at $\tilde{r} = 1$. This singularity implies a breakdown of the Hertzian theory over the width $\delta(\lambda)$, because the height and pressure profiles in our lubrication problem must remain smooth everywhere. In this region, the height scaling from Eq. (2) does not apply because the relevant lateral length scale is no longer l_H.

To capture the anomalous scaling of the height in the neck region and the width $\delta(\lambda)$, we take inspiration from the numerical collapse of Fig. 3. The key observation is that in the contact region under the solid ($\tilde{r} \ll 1$), the pressure is given by the Hertzian solution at leading order in the parameter λ [Fig. 3(b)]. By the same logic, when $\tilde{r} \gg 1$, the height is asymptotically Hertzian [Fig. 3(a)]. Using the lubrication equation (3), we construct the corresponding height and pressure solutions in each region. These solutions patch together over the neck region, shown schematically in the inset of Fig. 1(b). In the neck, both pressure and height vanish as some unknown power of λ; we denote the height scaling as $\phi_n(\lambda)$ and the pressure scaling as $\psi_n(\lambda)$. The patching conditions, derived in the SM [34], simultaneously determine $\delta(\lambda)$, $\phi_n(\lambda)$, and $\psi_n(\lambda)$, to give a complete set of scaling laws:

$$\begin{aligned} \delta(\lambda) = \lambda^{3/16},\ \phi_c(\lambda) = \lambda^{1/4}, \\ \psi_n(\lambda) = \lambda^{3/32},\ \phi_n(\lambda) = \lambda^{9/32}. \end{aligned} \tag{6}$$

In the insets of Fig. 3, we show that the scalings Eq. (6) now collapse our simulation data in the neck region as well as the contact region. Our asymptotic theory gives a new prediction: once re-dimensionalized, the relation $\phi_n(\lambda) = \lambda^{9/32}$ yields the anomalous neck height scaling

$$h \sim \Pi_0^{9/32} E^{-7/24} F^{1/96} R^{5/12}. \tag{7}$$

Again taking the load to go as the volume, $F \sim R^3$, we find the neck height scaling $h \sim R^{43/96}$. In Fig. 2, we show that these revised scalings with radius R and modulus E agree well with simulations. Taken together, the scalings Eqs. (2) and (7) provide a complete picture of elastic Leidenfrost floating.

We now ask about the limits of validity of our theory: when does the universality of the elastic Leidenfrost number λ break down? We first consider the vapor. The lubrication approximation made in Eq. (3) requires $h/l \ll 1$. As $R \to \infty$, using the contact height scaling $h \sim R^{7/12}$ gives $h/l_H \sim R^{-3/4}$, and so the lubrication approximation improves as we go further into the

Hertzian limit, even as the gap height increases. In this same limit, we expect deviations due to the breakdown of Hertz theory, which assumes that the Hertzian length scale l_H is much smaller than the sphere radius R, i.e., $l_H/R \ll 1$. Such deviations are visible in Fig. 3(b): the pressure profile does not asymptote to the exact Hertzian solution, there is a small systematic offset near $\tilde{r} = 0$. In the SM [34], we show that such deviations vanish when λ is fixed, while $l_H/R \to 0$. For $\lambda = 10^{-8}$ in Fig. 3(b), we have $l_H/R \approx 1/4$. Nevertheless, our Hertzian theory continues to provide quantitatively accurate predictions, even up to these relatively large values of the ratio l_H/R.

We have provided a fundamental description of elastic Leidenfrost floating, unraveling how the gap height interpolates between rigid and Hertzian regimes. To quantify this crossover, we have defined a dimensionless elastic Leidenfrost number λ. Our results provide the theoretical groundwork for interpreting recent experimental studies [1, 3], as well as several implications for future directions.

Using hydrogel spheres of radius $R = 7\,\mathrm{mm}$ and modulus $E = 50\,\mathrm{kPa}$, Ref. [3] measures average gap height against time in the floating regime. These experiments [3] place an upper bound on the early-time gap height as $h < (25 \pm 10)\,\mu\mathrm{m}$. Over longer times, inhomogeneous evaporation is observed to alter the solid's reference geometry. Our theory predicts a contact height of $h = 15\,\mu\mathrm{m}$ and a neck height of $h = 12\,\mu\mathrm{m}$. Our estimate of $\lambda \sim 10^{-5}$ places these experiments in the regime of Hertzian scaling. Taken together, we expect our results to provide a valuable counterpart to future experimental studies on floating behavior. Although our results are focused on the floating regime, they have implications for the observed spontaneous bouncing [1, 2]. Floating provides a reference stationary state against which bouncing dynamics can be compared.

Broadly, our work points towards combining Leidenfrost-type physics and soft elasticity beyond the experimental setup shown in Fig. 1(a). In soft lubrication theory, lift forces are generated by an imposed lateral motion of the solid [24, 26]. Motion could be induced either by global rotation of the soft solid [40, 41], or by placing it on an inclined plane [42]. For a Leidenfrost solid, these motion-induced forces will compete with those arising from phase change, and their interplay may allow for the tuning of gap height, or controllably inducing a float-to-bounce transition. Another broad consequence of our work is the importance of soft-solid geometry. As we show in the SM [34], an elastic cylinder has a distinct gap height scaling to the spherical case: for a cylinder in the Hertzian regime, we find a contact height scaling $h \sim R^{5/8}$. We envision tailoring the precise float height and configuration of an object by tuning its initial geometry—shape control which would not be possible for liquid droplets.

J.B. and A.S. acknowledge the support of the Engineering and Physical Sciences Research Council (EPSRC) through New Investigator Award No. EP/T000961/1. A.S. acknowledges the support of Royal Society under grant No. RGS/R2/202135. J.E.S. acknowledges EPSRC Grants No. EP/N016602/1, EP/S022848/1, EP/S029966/1, and EP/P031684/1.

* Electronic address: A.Souslov@bath.ac.uk

[1] S. R. Waitukaitis, A. Zuiderwijk, A. Souslov, C. Coulais, and M. van Hecke, Nature Physics **13**, 1095 (2017).
[2] J. T. Pham, M. Paven, S. Wooh, T. Kajiya, H.-J. Butt, and D. Vollmer, Nature Communications **8**, 905 (2017).
[3] S. Waitukaitis, K. Harth, and M. van Hecke, Physical Review Letters **121**, 048001 (2018).
[4] H. K. Khattak, P. Bianucci, and A. D. Slepkov, Proceedings of the National Academy of Sciences **116**, 4000 (2019).
[5] H. K. Khattak, S. R. Waitukaitis, and A. D. Slepkov, Soft Matter **15**, 5804 (2019).
[6] A.-L. Biance, C. Clanet, and D. Quéré, Physics of Fluids **15**, 1632 (2003).
[7] F. Celestini, T. Frisch, and Y. Pomeau, Physical Review Letters **109**, 034501 (2012).
[8] J. Burton, A. Sharpe, R. Van Der Veen, A. Franco, and S. Nagel, Physical Review Letters **109**, 074301 (2012).
[9] D. Quéré, Annual Review of Fluid Mechanics **45**, 197 (2013).
[10] B. Sobac, A. Rednikov, S. Dorbolo, and P. Colinet, Physical Review E **90**, 053011 (2014).
[11] H. Linke, B. Alemán, L. Melling, M. Taormina, M. Francis, C. Dow-Hygelund, V. Narayanan, R. Taylor, and A. Stout, Physical Review Letters **96**, 154502 (2006).
[12] G. Graeber, K. Regulagadda, P. Hodel, C. Küttel, D. Landolf, T. M. Schutzius, and D. Poulikakos, Nature Communications **12**, 1 (2021).
[13] T. Tran, H. J. Staat, A. Prosperetti, C. Sun, and D. Lohse, Physical Review Letters **108**, 036101 (2012).
[14] H. Van Dam, Reports on Progress in Physics **55**, 2025 (1992).
[15] I. U. Vakarelski, N. A. Patankar, J. O. Marston, D. Y. Chan, and S. T. Thoroddsen, Nature **489**, 274 (2012).
[16] G. Dupeux, M. Le Merrer, G. Lagubeau, C. Clanet, S. Hardt, and D. Quéré, Europhysics Letters **96**, 58001 (2011).
[17] G. Dupeux, T. Baier, V. Bacot, S. Hardt, C. Clanet, and D. Quéré, Physics of Fluids **25**, 051704 (2013).
[18] G. G. Wells, R. Ledesma-Aguilar, G. McHale, and K. Sefiane, Nature Communications **6**, 1 (2015).
[19] C. J. Hooke and J. P. O'Donoghue, Journal of Mechanical Engineering Science **14**, 34 (1972).
[20] B. J. Hamrock and D. Dowson, Journal of Lubrication Technology **98**, 223 (1976).
[21] J. Archard, Journal of Mechanical Engineering Science **10**, 165 (1968).
[22] K. Johnson, Journal of Mechanical Engineering Science **12**, 9 (1970).
[23] B. J. Hamrock, S. R. Schmid, and B. O. Jacobson, *Fundamentals of Fluid Film Lubrication* (Marcel Dekker, 2004).
[24] J. M. Skotheim and L. Mahadevan, Physical Review Let-

ters **92**, 245509 (2004).
[25] J. H. Snoeijer, J. Eggers, and C. H. Venner, Physics of Fluids **25**, 101705 (2013).
[26] M. H. Essink, A. Pandey, S. Karpitschka, C. H. Venner, and J. H. Snoeijer, Journal of Fluid Mechanics **915**, A49 (2021).
[27] J. A. Greenwood, Lubricants **8**, 51 (2020).
[28] C. Duprat and H. A. Shore, *Fluid-Structure Interactions in Low-Reynolds-Number Flows* (Royal Society of Chemistry, 2015).
[29] T. Gervais, J. El-Ali, A. Günther, and K. F. Jensen, Lab on a Chip **6**, 500 (2006).
[30] I. C. Christov, V. Cognet, T. C. Shidhore, and H. A. Stone, Journal of Fluid Mechanics **841**, 267 (2018).
[31] S. Leroy, A. Steinberger, C. Cottin-Bizonne, F. Restagno, L. Léger, and E. Charlaix, Physical Review Letters **108**, 264501 (2012).
[32] V. Bertin, Y. Amarouchene, E. Raphael, and T. Salez, arXiv:2104.00900 (2021).
[33] A. Kargar-Estahbanati and B. Rallabandi, Physical Review Fluids **6**, 034003 (2021).
[34] *Supplementary Material*.
[35] L. Landau and E. Lifshitz, *Theory of Elasticity* (Elsevier Science, 1986).
[36] K. L. Johnson, *Contact Mechanics* (Cambridge University Press, 1985).
[37] E. J. Bissett, Proceedings of the Royal Society of London. A. Mathematical and Physical Sciences **424**, 393 (1989).
[38] M. V. Chubynsky, K. I. Belousov, D. A. Lockerby, and J. E. Sprittles, Physical Review Letters **124**, 084501 (2020).
[39] I. Chakraborty, M. V. Chubynsky, and J. E. Sprittles, Journal of Fluid Mechanics **936**, A12 (2022).
[40] A. Bouillant, T. Mouterde, P. Bourrianne, A. Lagarde, C. Clanet, and D. Quéré, Nature Physics **14**, 1188 (2018).
[41] R. Brandão and O. Schnitzer, Physical Review Fluids **5**, 091601 (2020).
[42] B. Saintyves, T. Jules, T. Salez, and L. Mahadevan, Proceedings of the National Academy of Sciences **113**, 5847 (2016).